J. Korean Math. Soc. **54** (2017), No. 1, pp. 141–175
https://doi.org/10.4134/JKMS.j150616
pISSN: 0304-9914 / eISSN: 2234-3008

A HIGH-RESOLUTION VAN LEER-TYPE SCHEME FOR A MODEL OF FLUID FLOWS IN A NOZZLE WITH VARIABLE CROSS-SECTION

Dao Huy Cuong and Mai Duc Thanh

Abstract. We present a high-resolution van Leer-type numerical scheme for the isentropic model of fluid flows in a nozzle with variable cross-section. Basically, the scheme is an improvement of the Godunov-type scheme. The scheme is shown to be well-balanced, as it can capture exactly equilibrium states. Numerical tests are conducted which include comparisons between the van Leer-type scheme and the Godunov-type scheme. It is shown that the van Leer-type scheme achieves a very good accuracy for initial data belong to both supersonic and supersonic regions, and the exact solution eventually possesses a resonant phenomenon.

1. Introduction

In this paper we aim to construct a van Leer-type numerical scheme for the following isentropic model of fluid flows in a nozzle with variable cross-section

$$\begin{aligned} &\partial_t(a\rho) + \partial_x(a\rho u) = 0,\\ &\partial_t(a\rho u) + \partial_x(a(\rho u^2 + p)) = p\partial_x a, \quad x \in \mathbb{R}, \quad t > 0, \end{aligned} \tag{1.1}$$

where $\rho(x,t)$, $u(x,t)$, $p(x,t)$ denote the density, particle velocity, and pressure of the fluid, respectively, and $a = a(x)$ denotes the cross-section of the nozzle. The system (1.1) describes the balance of mass and the balance of momentum.

The nonconservative term on the right-hand side of the system (1.1) represents the effects of the geometry of the nozzle. It has been known that, by supplementing (1.1) with a trivial equation

$$\partial_t a = 0, \tag{1.2}$$

Received October 10, 2015; Revised June 2, 2016.
2010 *Mathematics Subject Classification.* Primary 35L65, 74XX; Secondary 76N10, 76L05.
Key words and phrases. shock wave, nonconservative, numerical approximation, Riemann problem, Godunov scheme, van Leer scheme, accuracy.
This research is funded by Vietnam National University HoChiMinh City (VNU-HCM) under grant number B2015-28-02.

one can transform (1.1) to a hyperbolic system of balance laws in nonconservative form

$$\partial_t U + A(U)\partial_x U = 0, \tag{1.3}$$

where $U = (\rho, u, a)$, and the matrix $A(U)$ is described later. Observe that the formulation of weak solutions of hyperbolic systems of balance laws in nonconservative form was introduced by [15]. Since this kind of systems can be used for the modeling of multi-phase flows, it has been intensively studied for many years. One of the most challenging problems for numerical approximations of nonconservative systems is that standard schemes often give unsatisfactory results. In particular, the errors may not be decreasing when the the mesh sizes tend to zero.

Motivated by our recent work [14] on a Godunov-type scheme for the model (1.1), we develop in this paper a high-resolution van Leer-type scheme. Observe that in the classical case of hyperbolic systems of conservation laws, van Leer's scheme is a second-order method and it is an improvement of the first-order Godunov' scheme. Many numerical tests are conducted for all types of initial data, where we compare the accuracy, the order of convergence of both schemes. These tests indicate that our van Leer-type scheme can give good approximations for exact solutions not only when the initial data are located in each subsonic or supersonic region, but also in both regions. It is very interesting that the scheme can eventually approximate very well the exact solution in the resonant case, where the exact solution contains colliding waves. This is in fact an important advantage of the van Leer-type scheme over many existing schemes. Furthermore, we show that the van Leer-type scheme is well-balanced, since it can capture exactly equilibrium states. Numerical tests show that this scheme has a much better accuracy than the Godunov-type scheme. However, tests also indicate that the van Leer-type scheme for the nonconservative system (1.1) may not be of second-order methods.

We note that numerical approximations of solutions of nonconservative hyperbolic systems of balance laws have attracted the attention of many authors. The reader is referred to [5, 13, 14, 22, 23] for numerical schemes for models of fluid flows in a nozzle with variable cross-section, to [8, 18, 16, 26] for numerical approximations of solutions of shallow water equations, to [3, 6, 7] for well-balanced numerical schemes for a single conservation law with source term, to [1, 4, 9, 10, 12, 28, 33, 35, 36] for numerical schemes for two-phase flow models. The Godunov-type schemes for hyperbolic systems of balance laws in nonconservative forms are constructed in [2, 14, 26, 30, 29]. The Riemann problem for models of fluid flows in a nozzle with discontinuous cross-section were studied in [19, 20, 24, 27, 31]. The Riemann problem for other hyperbolic systems in nonconservative form were considered in [17, 21, 25, 26, 32, 34]. See also the references therein.

The organization of this paper is as follows. Section 2 provides us with basic properties of the system (1.1)-(1.2). Section 3 is devoted to the exact Riemann

solvers for (1.1)-(1.2), where we provide computing algorithms for the exact solutions. In Section 4 we will construct a van Leer-type scheme for (1.1), after giving a review on the Godunov-type scheme. In Section 5 we present numerical tests for various cases of data. Finally, in Section 6 we make conclusions and discussions.

2. Preliminaries

2.1. Nonstrict hyperbolicity

In this paper, we assume that the pressure is given by an equation of state of an isentropic ideal gas

$$p = p(\rho) = \kappa\rho^\gamma,$$

where $\kappa > 0$, $1 < \gamma < 5/3$ are constant. Set

$$c = \sqrt{p'(\rho)}.$$

The system (1.1)-(1.2) for any smooth solution $U = (\rho, u, a)^T$ can be re-written in the nonconservative form as

$$\partial_t U + A(U)\partial_x U = 0, \tag{2.1}$$

where

$$A(U) = \begin{pmatrix} u & \rho & \frac{\rho u}{a} \\ \frac{c^2}{\rho} & u & 0 \\ 0 & 0 & 0 \end{pmatrix}.$$

The matrix $A(U)$ admits the following three eigenvalues

$$\lambda_1 = u - c, \quad \lambda_2 = u + c, \quad \lambda_3 = 0. \tag{2.2}$$

The corresponding eigenvectors can be chosen as

$$r_1 = \begin{pmatrix} \rho \\ -c \\ 0 \end{pmatrix}, \quad r_2 = \begin{pmatrix} \rho \\ c \\ 0 \end{pmatrix}, \quad r_3 = \begin{pmatrix} -\rho u^2 \\ uc^2 \\ a(u^2 - c^2) \end{pmatrix}.$$

The first and the third characteristic speeds coincide on the *upper sonic surface*:

$$\mathcal{C}^+ = \{U : \lambda_1(U) = \lambda_3(U)\} = \{(\rho, u, a) : u = c\}.$$

The second and the third characteristic speeds coincide on the *lower sonic surface*:

$$\mathcal{C}^- = \{U : \lambda_2(U) = \lambda_3(U)\} = \{(\rho, u, a) : u = -c\}.$$

Thus, the system (1.1)-(1.2) is strictly hyperbolic on following regions:

$$G_1 = \{U : \lambda_1(U) > \lambda_3(U)\} = \{(\rho, u, a) : u > c\},$$
$$G_2 = \{U : \lambda_1(U) < \lambda_3(U) < \lambda_2(U)\} = \{(\rho, u, a) : |u| < c\},$$
$$G_2^+ = \{U(\rho, u, a) \in G_2 : u > 0\}, \quad G_2^- = \{U(\rho, u, a) \in G_2 : u < 0\},$$
$$G_3 = \{U : \lambda_2(U) < \lambda_3(U)\} = \{(\rho, u, a) : u < -c\}.$$

The set $G_1 \cup G_3$ is called the *supersonic region*, while G_2 is called the *subsonic region*. The third characteristic field is *linearly degenerate*, since

$$\nabla\lambda_3 \cdot r_3 = 0.$$

The first and the second characteristic fields are *genuinely nonlinear*, since

$$-\nabla\lambda_1 \cdot r_1 = \nabla\lambda_2 \cdot r_2 = \frac{(\gamma+1)c}{2} > 0.$$

2.2. Shock wave curves

The Rankine-Hugoniot relation for a shock wave corresponding to the equation (1.2) is given by

$$-\sigma[a] = 0,$$

where σ denotes the speed of the shock, $[a] = a_R - a_L$ is the jump of the quantity a. As discussed in [24], across a discontinuity there are two possibilities:

(i) either the cross-section a remains constant,
(ii) or the discontinuity is stationary (i.e., the shock propagates with zero speed).

Let us consider the first the case (i). Recall that a *shock wave* of (1.1)-(1.2) connecting a left-hand state U_L to a right-hand state U_R is a weak solution of the form

$$U_{shock}(x,t;U_L,U_R) = \begin{cases} U_L, & x < \sigma t, \\ U_R, & x > \sigma t, \end{cases} \tag{2.3}$$

where $\sigma = \sigma(U_L, U_R)$ is the shock speed. A shock wave (2.3) is *admissible*, called an i-Lax shock, if it satisfies the Lax shock inequalities,

$$\lambda_i(U_R) < \sigma(U_L,U_R) < \lambda_i(U_L), \quad i = 1,2.$$

From now on, we consider admissible shock waves, only. The Rankine-Hugoniot relations associated the first and second equation of (1.1)-(1.2) are given by

$$\begin{aligned} -\sigma[\rho] + [\rho u] &= 0, \\ -\sigma[\rho u] + [\rho(u^2+p)] &= 0, \end{aligned}$$

where $[A] = A_R - A_L$ is the jump of the quantity A. By canceling σ from above system, we obtain the Hugoniot locus

$$(u_L - u_R)^2 = -(p_L - p_R)\Big(\frac{1}{\rho_L} - \frac{1}{\rho_R}\Big). \tag{2.4}$$

The Lax shock inequalities yield the following

- For $1-$Lax shock:

$$u_L > u_R, \quad \rho_L < \rho_R; \tag{2.5}$$

- For $2-$Lax shock:

$$u_L > u_R, \quad \rho_L > \rho_R. \tag{2.6}$$

From (2.4) and (2.5), the forward curve of 1-shock waves consisting of all right-hand states U that can be connected to a given left-hand state U_0 by an 1-Lax shock is given by

$$\mathcal{S}_1(U_0): \quad u = u_0 - \sqrt{-(p-p_0)\Big(\frac{1}{\rho}-\frac{1}{\rho_0}\Big)}, \quad \rho > \rho_0.$$

From (2.4) and (2.5), the backward curve of 1-shock waves consisting of all left-hand states U that can be connected to a given right-hand state U_0 by an 2-Lax shock is given by

$$\mathcal{S}_2^B(U_0): \quad u = u_0 + \sqrt{-(p-p_0)\Big(\frac{1}{\rho}-\frac{1}{\rho_0}\Big)}, \quad \rho > \rho_0.$$

Furthermore, it has been shown in [24] that the shock speeds may vanish. Precisely, we have the following result.

Lemma 2.1. (i) *The 1-shock speed $\sigma_1(U_0,U)$ may change sign along the 1-shock wave curve $\mathcal{S}_1(U_0)$. More precisely, if $U_0 \in G_2 \cup G_3$, then $\sigma_1(U_0,U)$ remains negative*:

$$\sigma_1(U_0,U) < 0, \quad U \in \mathcal{S}_1(U_0).$$

If $U_0 \in G_1$, then there is exactly one state, denoted by $U_0^{\#} \in \mathcal{S}_1(U_0) \cap G_2^+$, such that

$$\begin{aligned} &\sigma_1(U_0,U_0^{\#}) = 0,\\ &\sigma_1(U_0,U) > 0, \quad \rho_0 < \rho < \rho_0^{\#},\\ &\sigma_1(U_0,U) < 0, \quad \rho > \rho_0^{\#}. \end{aligned}$$

(ii) *The 2-shock speed $\sigma_2(U,U_0)$ may change sign along the 2-shock wave backward curve $\mathcal{S}_2^B(U_0)$. More precisely, if $U_0 \in G_1 \cup G_2$, then $\sigma_2(U,U_0)$ remains positive*:

$$\sigma_2(U,U_0) > 0, \quad U \in \mathcal{S}_2^B(U_0).$$

If $U_0 \in G_3$, then there is exactly one state $U_0^{@} \in \mathcal{S}_2(U_0) \cap G_2^-$, such that

$$\begin{aligned} &\sigma_2(U_0^{@},U_0) = 0,\\ &\sigma_2(U,U_0) < 0, \quad \rho_0 < \rho < \rho_0^{@},\\ &\sigma_2(U,U_0) > 0, \quad \rho > \rho_0^{@}. \end{aligned}$$

2.3. Rarefaction wave curves

Rarefaction waves are piecewise smooth self-similar solutions of (1.1)-(1.2) associated with non-linear characteristic fields, which have the form

$$U_{rare}(x,t) = V(\xi), \quad \xi = \frac{x}{t}, \quad x \in \mathbb{R},\ t > 0.$$

Substituting this into (2.1), we can see that rarefaction waves are solutions of following initial-value problem for ODEs

$$\begin{aligned}&\frac{dV(\xi)}{d\xi} = \frac{1}{\nabla\lambda_i(V(\xi))\cdot r_i(V(\xi))} r_i(V(\xi)), \quad \xi \geq \lambda_i(U_0),\\ &V(\lambda_i(U_0)) = U_0, \quad i = 1, 2.\end{aligned}$$

Therefore, a rarefaction wave satisfies the following ordinary differential equations

$$\begin{aligned}\rho'(\xi) &= -\frac{2\rho}{(\gamma+1)c} \quad \text{for} \quad i = 1,\\ \rho'(\xi) &= \frac{2\rho}{(\gamma+1)c} \quad \text{for} \quad i = 2,\\ u'(\xi) &= \frac{2}{\gamma+1},\\ a'(\xi) &= 0,\end{aligned}$$

where $(\cdot)' = d/d\xi$. The last equation implies that the cross-section a remains constant through any rarefaction fan. Moreover, the i-rarefaction wave of (1.1)-(1.2) connecting a left-hand state U_L to a right-hand state U_R (with $a_L = a_R$) is given by

$$U_{r_i}(x,t;U_L,U_R) = \begin{cases} U_L, & \dfrac{x}{t} < \lambda_i(U_L),\\ \Big(\rho_{r_i}(x,t), u_{r_i}(x,t)\Big), & \lambda_i(U_L) \leq \dfrac{x}{t} \leq \lambda_i(U_R),\\ U_R, & \dfrac{x}{t} > \lambda_i(U_R),\end{cases}$$

where

$$\begin{aligned}&(\rho_{r_i}(x,t))^{\frac{\gamma-1}{2}} - (\rho_L)^{\frac{\gamma-1}{2}} = (-1)^i \frac{\gamma-1}{(\gamma+1)\sqrt{\kappa\gamma}}\Big(\frac{x}{t} - \lambda_i(U_L)\Big),\\ &u_{r_i}(x,t) - u_L = \frac{2}{\gamma+1}\Big(\frac{x}{t} - \lambda_i(U_L)\Big), \quad i = 1, 2.\end{aligned}$$

Given a left-hand state U_0, the set of all right-hand states that can be connected to U_0 by an 1-rarefaction waves of (1.1)-(1.2) forms a curve, denoted by $\mathcal{R}_1(U_0)$. In a backward way, given a right-hand state U_0, the set of all left-hand states that can be connected to U_0 by an 2-rarefaction wave forms a curve, denoted by $\mathcal{R}_2^B(U_0)$. These curves are given by

$$\begin{aligned}&\mathcal{R}_1(U_0): \quad u = u_0 - \frac{2\sqrt{\kappa\gamma}}{\gamma-1}(\rho^{(\gamma-1)/2} - \rho_0^{(\gamma-1)/2}), \quad \rho \leq \rho_0,\\ &\mathcal{R}_2^B(U_0): \quad u = u_0 + \frac{2\sqrt{\kappa\gamma}}{\gamma-1}(\rho^{(\gamma-1)/2} - \rho_0^{(\gamma-1)/2}), \quad \rho \leq \rho_0,\end{aligned}$$

where $\rho \leq \rho_0$ follows from the condition $\lambda_i(U_L) \leq \lambda_i(U_R)$, see [24]. We can therefore define the forward and backward wave wave curves in the non-linear

characteristic fields as follows

$$\mathcal{W}_1(U_0) = \mathcal{R}_1(U_0) \cup \mathcal{S}_1(U_0),$$
$$\mathcal{W}_2^B(U_0) = \mathcal{R}_2^B(U_0) \cup \mathcal{S}_2^B(U_0).$$

As seen above, the curves $\mathcal{W}_1(U_0)$ can be parameterized as a function $u = w_1(U_0;\rho)$ of $\rho > 0$, and the curves $\mathcal{W}_2^B(U_0)$ can be parameterized as a function $u = w_2^B(U_0;\rho)$ of $\rho > 0$. It was shown in [24] that $w_1(U_0;\rho)$ *is strictly convex and strictly decreasing functions of* $\rho > 0$, *while* $w_2^B(U_0;\rho)$ *is strictly concave and strictly increasing functions of* $\rho > 0$.

2.4. Stationary waves

Let us now consider the case (ii), where the discontinuity satisfies the jump relations

$$\begin{aligned} &[a\rho u] = 0, \\ &\left[\frac{u^2}{2} + \frac{c^2}{\gamma - 1}\right] = 0, \end{aligned} \tag{2.7}$$

see [24]. In this case, the shock wave connecting two states $U_\pm$ is called the *stationary wave*. $U_\pm$ are called two *equilibrium states*.

Let $U = (\rho, u, a)$ and $U_0 = (\rho_0, u_0, a_0)$ be the two equilibrium states on both sides of a stationary wave satisfying (2.7). Set

$$\mu = \frac{2\kappa\gamma}{\gamma - 1}.$$

Assuming that U_0, a_0 and a are fixed. By substituting $u = a_0\rho_0 u_0/a\rho$ from the first equation of (2.7) into the second of equation (2.7), we have the following nonlinear equation in ρ:

$$F(\rho) = F(\rho; U_0, a_0, a) := -\mu\rho^{\gamma+1} + (u_0^2 + \mu\rho_0^{\gamma-1})\rho^2 - (a_0 u_0 \rho_0/a)^2 = 0.$$

The domain of the function F is given by

$$0 < \rho \le \bar{\rho}(U_0) := \Big(\frac{1}{\mu}u_0^2 + \rho_0^{\gamma-1}\Big)^{\frac{1}{\gamma-1}}.$$

We have

$$F'(\rho) = -\mu(\gamma+1)\rho^\gamma + 2(u_0^2 + \mu\rho_0^{\gamma-1})\rho.$$

Therefore

$$\begin{aligned} &F'(\rho) < 0, \quad \rho_{\max} < \rho < \bar{\rho}, \\ &F'(\rho) > 0, \quad 0 < \rho < \rho_{\max}, \end{aligned}$$

where

$$\rho_{\max} = \rho_{\max}(U_0) := \left(\frac{2}{\mu(\gamma+1)}\left(u_0^2 + \mu\rho_0^{\gamma-1}\right)\right)^{\frac{1}{\gamma-1}}.$$

The function $\rho \mapsto F(\rho)$ takes negative values at the end-points. Thus, it admits some root if and only if the maximum value is non-negative. This is equivalent to saying that

$$a \geq a_{\min}(U_0) := \frac{a_0\rho_0|u_0|}{\sqrt{\kappa\gamma}(\rho_{\max})^{\frac{\gamma+1}{2}}}.$$

Thus, given U_0, a stationary wave connecting from U_0 to some state $U = (\rho, u, a)$ exists if and only if $a \geq a_{\min}(U_0)$. Moreover, if $a > a_{\min}(U_0)$, then there are exactly two values $\rho^{smaller} < \rho_{\max} < \rho^{bigger}$ such that

$$F(\rho^{smaller}) = F(\rho^{bigger}) = 0.$$

The following lemma characterizes the stationary waves.

Lemma 2.2 (Lem. 2.3, [24])**.** *The following conclusions hold.*

a)

$$\begin{aligned}
&\rho_{\max}(U_0) > \rho_0, \quad U_0 \in G_1 \cup G_3,\\
&\rho_{\max}(U_0) < \rho_0, \quad U_0 \in G_2,\\
&\rho_{\max}(U_0) = \rho_0, \quad U_0 \in \mathcal{C}^{\pm}.
\end{aligned}$$

b) *The state*

$$U^s = SW^{smaller}(U_0, a_0, a) := \Big(\rho^{smaller}, \frac{a_0\rho_0u_0}{a\rho^{smaller}}, a\Big)$$

belongs to G_1 if $u_0 > 0$, and belongs to G_3 if $u_0 < 0$, while the state

$$U^b = SW^{bigger}(U_0, a_0, a) := \Big(\rho^{bigger}, \frac{a_0\rho_0u_0}{a\rho^{bigger}}, a\Big)$$

always belongs to G_2. In addition, it holds that

(i) *If $a > a_0$, then*

$$\rho^{smaller} < \rho_0 < \rho^{bigger}.$$

(ii) *If $a < a_0$, then*

$$\begin{aligned}
&\rho_0 < \rho^{smaller} \quad \textit{for} \quad U_0 \in G_1 \cup G_3,\\
&\rho_0 > \rho^{bigger} \quad \textit{for} \quad U_0 \in G_2.
\end{aligned}$$

It follows from Lemma 2.2 that there are two possible stationary waves $SW^{smaller}(U_0, a_0, a)$, $SW^{bigger}(U_0, a_0, a)$ from a given state U_0 to a state with a new level cross-section a. Thus, it is necessary to impose some condition to select a unique physical stationary as follows.

(MC) Any stationary jump must not cross the sonic curve in the (ρ, u)-plane.

3. The computational Riemann solvers

In this section, we use some following notations:

(i) $W_k(U_i, U_j)$ ($S_k(U_i, U_j), R_k(U_i, U_j)$) denotes the kth-wave (kth-shock, kth-rarefaction wave, respectively) connecting the left-hand state U_i to the right-hand state U_j, $k = 1, 2, 3$.
(ii) $W_m(U_i, U_j) \oplus W_n(U_j, U_k)$ indicates that there is an mth-wave from the left-hand state U_i to the right-hand state U_j, followed by an nth-wave from the left-hand state U_j to the right-hand state U_k, $m, n \in \{1, 2, 3\}$.
(iii) $U_0^{\#}$ denotes the state on the shock wave curve $\mathcal{S}_1(U_0)$ such that $\sigma_1(U_0, U_0^{\#}) = 0$.
(iv) $U_0^{@}$ denotes the state on the backward shock wave curve $\mathcal{S}_2^B(U_0)$ such that $\sigma_2(U_0^{@}, U_0) = 0$.
(v) $U_0^s = SW^{smaller}(U_0, a_0, a), U_0^b = SW^{bigger}(U_0, a_0, a)$ denote the states resulted by stationary contact wave from U_0.
(vi) $U^{\pm} = \mathcal{W}_1(U_L) \cap \mathcal{C}^{\pm}$; $V^{\pm} = \mathcal{W}_2^B(U_R) \cap \mathcal{C}^{\pm}$.

3.1. Case A: $U_L \in G_1$

Construction A1: The Riemann solution begins with a stationary contact wave from U_L to U_L^s. By Lemma 2.1, there is one state $U_L^{s\#}$ such that the shock speed $\sigma_1(U_L^s, U_L^{s\#}) = 0$ and $\sigma_1(U_L^s, U) > 0$ for $\rho_L^s < \rho < \rho_L^{s\#}$, $\sigma_1(U^s, U) < 0$ for $\rho > \rho_L^{s\#}$. So, the next part of the solution is a 1-wave from U^s to state $U(\rho, u)$ such that $0 < \rho \le \rho_L^{s\#}$. The set of these states U forms the curve composite $\mathcal{W}_{31}(U_L, a_R)$. For example, see the blue curve in Figure 1. Observe that $\mathcal{W}_{31}(U_L, a_R)$ is a part of the curve $\mathcal{W}_1(U_L^s)$. If the curve $\mathcal{W}_2^B(U_R)$ intersects the curve $\mathcal{W}_{31}(U_L, a_R)$ at a point U_1, then the Riemann problem of (1.1)-(1.2) admits a solution of the form

$$W_3(U_L, U_L^s) \oplus W_1(U_L^s, U_1) \oplus W_2(U_1, U_R). \tag{3.1}$$

Remark 3.1. If

$$\max\{\lambda_1(U_L^s), \lambda_1(U_1)\} \le \min\{\lambda_2(U_1), \lambda_2(U_R)\} \text{ and } a_R > a_{\min}(U_L),$$

then the solution (3.1) makes sense.

Computational algorithm for Construction A1: We sketch to compute the point U_1 as follows.

- Step 1: Set $\rho_1 = 0$, $\rho_2 = \rho_L^{s\#}$;
- Step 2: Compute $\rho = \dfrac{\rho_1 + \rho_2}{2}$, $u = w_1(U_L^s; \rho)$ and set $U_1 = (\rho, u)$;
- Step 3:
  - If U_1 belongs to $\mathcal{W}_2^B(U_R)$, end;
  - If U_1 is above $\mathcal{W}_2^B(U_R)$, then set $\rho_1 = \rho$ and return Step 2;
  - If U_1 is below $\mathcal{W}_2^B(U_R)$, then set $\rho_2 = \rho$ and return Step 2.

Construction A2: For each level a between a_L and a_R, the Riemann solution can begin with the stationary contact wave from U_L to $U_L^s = SW^{smaller}(U_L, a_L, a)$. The next part of the solution is a 1-shock from state U_L^s to state $U_L^{s\#}$. Then, the next part of the solution is a stationary contact wave from $U_L^{s\#}$ to state $U_L^{s\#b} = SW^{bigger}(U_L^{s\#}, a, a_R)$. The set of such states $U_L^{s\#b}$ forms the curve composite $\mathcal{W}_{313}(U_L, a_R)$. So, $U_L^{\#b}$ and $U_L^{s\#}$ are two endpoints of this curve. For example, see the black curve in Figure 1. If the curve $\mathcal{W}_2^B(U_R)$ intersects the curve $\mathcal{W}_{313}(U_L, a_R)$ at a point U_1, then the Riemann problem of (1.1)-(1.2) admits a solution of the form

$$W_3(U_L, U_L^s) \oplus S_1(U_L^s, U_L^{s\#}) \oplus W_3(U_L^{s\#}, U_1 = U_L^{s\#b}) \oplus W_2(U_1, U_R). \tag{3.2}$$

Remark 3.2. If U_1 belongs to the rarefaction part $\mathcal{R}_2(U_R)$, then the solution (3.2) makes sense if $a_R > a_{\min}(U_L)$. If U_1 belongs to the shock part $\mathcal{S}_2(U_R)$, then the solution (3.2) makes sense if $a_R > a_{\min}(U_L)$ and $\sigma_2(U_1, U_R) > 0$.

Computational algorithm for Construction A2: We sketch to compute the points U_L^s, $U_L^{s\#}$, $U_L^{s\#b}$ as follows. Assume to the end-point $U_L^{\#b}$ of the composite wave curve $\mathcal{W}_{313}(U_L, a_R)$ is located below $\mathcal{W}_2^B(U_R)$.

- Step 1: Set $a_1 = a_L$, $a_2 = a_R$;
- Step 2:
  - Compute $a = \dfrac{a_1 + a_2}{2}$;
  - Compute $U_L^s = SW^{smaller}(U_L, a_L, a)$;
  - Compute $U_L^{s\#}$;
  - Compute $U_L^{s\#b} = SW^{bigger}(U_L^{s\#}, a, a_R)$;
- Step 3:
  - If $U_L^{s\#b}$ belongs to $\mathcal{W}_2^B(U_R)$, end;
  - If $U_L^{s\#b}$ is above $\mathcal{W}_2^B(U_R)$, then set $a_2 = a$ and return Step 2;
  - If $U_L^{s\#b}$ is below $\mathcal{W}_2^B(U_R)$, then set $a_1 = a$ and return Step 2.

Construction A3: The Riemann solution begins with 1-shock to state U_1 such that $\sigma_1(U_L, U_1) \le 0$. So, U_1 is between $U_L^{\#}$ and U^-. The next part of the solution is a stationary contact wave from U_1 to state U_1^b. The set of such states U_1^b forms the curve composite $\mathcal{W}_{13}^{caseA}(U_L, a_R)$. Observe that $U_L^{\#b}$ and U^{-b} are two endpoints of this curve. For example, see the red curve in Figure 1. If the curve $\mathcal{W}_2^B(U_R)$ intersects the curve $\mathcal{W}_{13}^{caseA}(U_L, a_R)$ at a point U_2, then the Riemann problem of (1.1)-(1.2) admits a solution of the form

$$S_1(U_L, U_1) \oplus W_3(U_1, U_2) \oplus W_2(U_2, U_R). \tag{3.3}$$

Remark 3.3. If U_2 belongs to the rarefaction part $\mathcal{R}_2(U_R)$, then the solution (3.3) makes sense if $a_R > a_{\min}(U_L)$. If U_2 belongs to the shock part $\mathcal{S}_2(U_R)$, then the solution (3.3) makes sense if $a_R > a_{\min}(U_L)$ and $\sigma_2(U_2, U_R) > 0$.

Computational algorithm for Construction A3: We sketch to compute the points U_1, U_2 as follows.

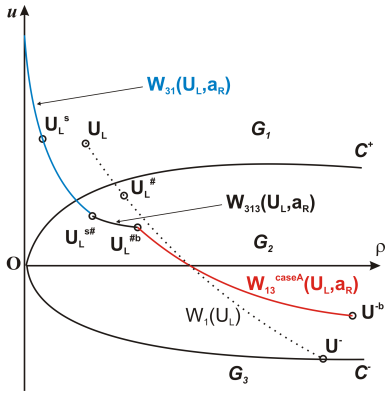

FIGURE 1. The composite wave curves $\mathcal{W}_{31}(U_L, a_R)$, $\mathcal{W}_{313}(U_L, a_R)$ and $\mathcal{W}_{13}^{caseA}(U_L, a_R)$ in the (ρ, u)-plane.

- Step 1: Set $\rho_1 = \rho_L^{\#}$, $\rho_2 = \rho^{-}$;
- Step 2:
  - Compute $\rho = \dfrac{\rho_1 + \rho_2}{2}$, $u = w_1(U_L; \rho)$ and set $U_1 = (\rho, u)$;
  - Compute $U_2 = SW^{bigger}(U_1, a_L, a_R)$;
- Step 3:
  - If U_2 belongs to $\mathcal{W}_2^B(U_R)$, end;
  - If U_2 is above $\mathcal{W}_2^B(U_R)$, then set $\rho_1 = \rho$ and return Step 2;
  - If U_2 is below $\mathcal{W}_2^B(U_R)$, then set $\rho_2 = \rho$ and return Step 2.

3.2. Case B: $U_L \in G_2$

Construction B1: The Riemann solution begins with a 1-rarefaction wave from U_L to U^+. The next part of the solution is a stationary wave from U^+ to the state U^{+s}. We know that there is one state $U^{+s\#}$ such that

$$\sigma_1(U^{+s}, U^{+s\#}) = 0.$$

So, the next part of the solution is a 1-wave from U^{+s} to U such that $0 < \rho \leq \rho^{+s\#}$. The set of U forms the composite curve $\mathcal{W}_{131}(U_L, a_R)$. Observe that $\mathcal{W}_{131}(U_L, a_R)$ is a part of the curve $\mathcal{W}_1(U^{+s})$. For example, see the blue curve in Figure 2. If the curve $\mathcal{W}_2^B(U_R)$ intersects the curve $\mathcal{W}_{131}(U_L, a_R)$ at a point U_1, then the Riemann problem of (1.1)-(1.2) admits a solution of the form

$$R_1(U_L, U^+) \oplus W_3(U^+, U^{+s}) \oplus W_1(U^{+s}, U_1) \oplus W_2(U_1, U_R). \tag{3.4}$$

Remark 3.4. If

$$\max\{\lambda_1(U^{+s}), \lambda_1(U_1)\} \leq \min\{\lambda_2(U_1), \lambda_2(U_R)\} \text{ and } a_R > a_{\min}(U_L),$$

then the solution (3.4) makes sense.

Computational algorithm for Construction B1: is similar to *Computational algorithm for Construction A1*, since the composite wave curve $\mathcal{W}_{131}(U_L, a_R)$ coincides with $\mathcal{W}_{31}(U^+, a_R)$.

Construction B2: For each level a between a_L and a_R, the Riemann solution begins with the 1-rarefaction wave to U^+. This rarefaction wave can be followed by a stationary contact wave U_+ to a state $U^{+s} = SW^{smaller}(U^+, a_L, a)$. The next part of the solution is a 1-shock wave from U^{+s} to the state $U^{+s\#}$. Then, the next part of the solution is a stationary contact wave from $U^{+s\#}$ to $U^{+s\#b} = SW^{bigger}(U^{+s}, a, a_R)$. The set of $U^{+s\#b}$ forms a curve composite, denoted by $\mathcal{W}_{1313}(U_L, a_R)$. Observe that $U^{+s\#}$ and U^{+b} are two endpoints of the curve composite $\mathcal{W}_{1313}(U_L, a_R)$. For example, see the black curve in Figure 2. If the curve $\mathcal{W}_2^B(U_R)$ intersects the curve $\mathcal{W}_{1313}(U_L, a_R)$ at a point U_1, then the Riemann problem of (1.1)-(1.2) admits a solution of the form

$$\begin{aligned} &R_1(U_L, U^+) \oplus W_3(U^+, U^{+s}) \oplus S_1(U^{+s}, U^{+s\#}) \\ &\qquad \oplus W_3(U^{+s\#}, U_1 = U^{+s\#b}) \oplus W_2(U_1, U_R). \end{aligned} \tag{3.5}$$

Remark 3.5. If U_1 belongs to the rarefaction part $\mathcal{R}_2(U_R)$, then the solution (3.5) makes sense if $a_R > a_{\min}(U_L)$. If U_1 belongs to the shock part $\mathcal{S}_2(U_R)$, then the solution (3.5) makes sense if $a_R > a_{\min}(U_L)$ and $\sigma_2(U_2, U_R) > 0$.

Computational algorithm for Construction B2: is similar to *Computational algorithm for Construction A2*, since the composite wave curve $\mathcal{W}_{1313}(U_L, a_R)$ coincides with $\mathcal{W}_{313}(U^+, a_R)$.

Construction B3: The Riemann solution begins with a 1-wave from U_L to state U_1 between U^+ and U^-. Then the next part of the solution is a stationary contact wave from U_1 to U_1^b. The set of such states U_1^b forms a curve composite, denoted by $\mathcal{W}_{13}^{caseB}(U_L, a_R)$. Observe that U^{-b} and U^{+b} be the two endpoints of this curve. For example, see the red curve in Figure 2. If the curve $\mathcal{W}_2^B(U_R)$ intersects the curve $\mathcal{W}_{13}^{caseB}(U_L, a_R)$ at a point U_2, then the Riemann problem of (1.1)-(1.2) admits a solution of the form

$$W_1(U_L, U_1) \oplus W_3(U_1, U_2) \oplus W_2(U_2, U_R). \tag{3.6}$$

Remark 3.6. If U_2 belongs to the rarefaction part $\mathcal{R}_2(U_R)$, then the solution (3.3) makes sense if $a_R > a_{\min}(U_L)$. If U_2 belongs to the shock part $\mathcal{S}_2(U_R)$, then the solution (3.3) makes sense if $a_R > a_{\min}(U_L)$ and $\sigma_2(U_2, U_R) > 0$.

Computational algorithm for Construction B3: is similar to the *Computational algorithm for Construction A3*, but one need to replace $\rho_1 = \rho_L^{\#}$ from Step 1 with $\rho_1 = \rho^+$.

3.3. Case C: $U_R \in G_3$

Construction C1: The Riemann solution begins backward with a stationary contact wave from U_R^s to U_R. By Lemma 2.1, there is one state $U_R^{s@}$ on the backward curve $\mathcal{S}_2^B(U_R^s)$ such that $\sigma_2(U_R^{s@}, U_R^s) = 0$ and $\sigma_2(U, U_R^s) < 0$ for $\rho_R^s <$

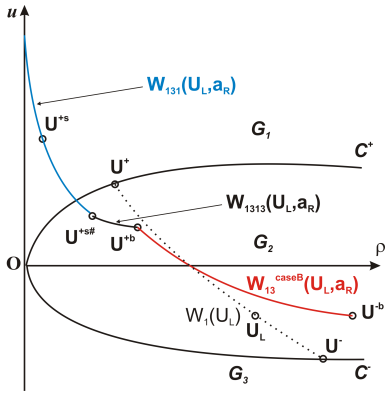

FIGURE 2. The composite wave curves $\mathcal{W}_{131}(U_L, a_R)$, $\mathcal{W}_{1313}(U_L, a_R)$ and $\mathcal{W}_{13}^{caseB}(U_L, a_R)$ in the (ρ, u)-plane.

$\rho < \rho_R^{s@}$, $\sigma_2(U, U_R^s) > 0$ for $\rho > \rho_R^{s@}$. So, the next backward part of the solution is a 2-wave from some state $U(\rho, u)$ to U_R^s such that $0 < \rho \leq \rho_R^{s@}$. The set of these states U forms the backward composite curve $\mathcal{W}_{32B}(U_R, a_L)$. Observe that $\mathcal{W}_{32B}(U_R, a_L)$ is a part of the curve $\mathcal{W}_2^B(U_R^s)$. For example, see the blue curve in Figure 3. If the curve $\mathcal{W}_1(U_L)$ intersects the curve $\mathcal{W}_{32B}(U_R, a_L)$ at a point U_1, then the Riemann problem of (1.1)-(1.2) admits a solution of the form

$$W_1(U_L, U_1) \oplus W_2(U_1, U_R^s) \oplus W_3(U_R^s, U_R). \tag{3.7}$$

Remark 3.7. If

$$\max\{\lambda_1(U_L), \lambda_1(U_1)\} \leq \min\{\lambda_2(U_1), \lambda_2(U_R^s)\} \text{ and } a_L > a_{\min}(U_R),$$

then the solution (3.7) makes sense.

Computational algorithm for Construction C1: We sketch to compute the point U_1 as follows.

- Step 1: Set $\rho_1 = 0$, $\rho_2 = \rho_R^{s@}$;
- Step 2: Compute $\rho = \dfrac{\rho_1 + \rho_2}{2}$, $u = w_2^B(U_R^s; \rho)$ and set $U_1 = (\rho, u)$;
- Step 3:
  - If U_1 belongs to $\mathcal{W}_1(U_L)$, end;
  - If U_1 is above $\mathcal{W}_1(U_L)$, then set $\rho_2 = \rho$ and return Step 2;
  - If U_1 is below $\mathcal{W}_1(U_L)$, then set $\rho_1 = \rho$ and return Step 2.

Construction C2: For each level a between a_L and a_R, the Riemann solution can begin backward with the stationary contact wave from $U_R^s = SW^{smaller}(UR, a_R, a)$ to U_R. The next backward part of the solution is a 2-shock from state $U_R^{s@}$ to state U_R^s. Then, the next backward part of the solution is a stationary contact wave from $U_R^{s@b} = SW^{bigger}(U_R^{s@}, a, a_L)$ to $U_R^{s@}$. The set of such states

$U_R^{s@b}$ forms the backward composite curve $\mathcal{W}_{323B}(U_R, a_L)$. So, $U_R^{@b}$ and $U_R^{s@}$ are two endpoints of this curve. For example, see the black curve in Figure 3. If the curve $\mathcal{W}_1(U_L)$ intersects the curve $\mathcal{W}_{323B}(U_R, a_L)$ at a point U_1, then the Riemann problem of (1.1)-(1.2) admits a solution of the form

$$W_1(U_L, U_1 = U_R^{s@b}) \oplus W_3(U_1, U_R^{s@}) \oplus S_2(U_R^{s@}, U_R^s) \oplus W_3(U_R^s, U_R). \tag{3.8}$$

Remark 3.8. If U_1 belongs to the rarefaction part $\mathcal{R}_1(U_L)$, then the solution (3.8) makes sense if $a_L > a_{\min}(U_R)$. If U_1 belongs to the shock part $\mathcal{S}_2(U_L)$, then the solution (3.8) makes sense if $a_L > a_{\min}(U_R)$ and $\sigma_1(U_L, U_1) < 0$.

Computational algorithm for Construction C2: We sketch to compute the points U_R^s, $U_R^{s@}$, $U_L^{s@b}$ as follows. Assume to the end-point $U_R^{@b}$ of the composite wave curve $\mathcal{W}_{323B}(U_R, a_L)$ is located above the wave curve $\mathcal{W}_1(U_L)$.

- Step 1: Set $a_1 = a_R$, $a_2 = a_L$;
- Step 2:
  - Compute $a = \dfrac{a_1 + a_2}{2}$;
  - Compute $U_R^s = SW^{smaller}(U_R, a_R, a)$;
  - Compute $U_R^{s@}$;
  - Compute $U_R^{s@b} = SW^{bigger}(U_R^{s@}, a, a_L)$;
- Step 3:
  - If $U_R^{s@b}$ belongs to $\mathcal{W}_1(U_L)$, end;
  - If $U_R^{s@b}$ is above $\mathcal{W}_1(U_L)$, then set $a_1 = a$ and return Step 2;
  - If $U_R^{s@b}$ is below $\mathcal{W}_1(U_L)$, then set $a_2 = a$ and return Step 2.

Construction C3: The Riemann solution begins backward with 2-shock from U_2 to U_R such that $\sigma_1(U_2, U_R) \geq 0$. So, U_2 is between $U_R^{@}$ and V^+. The next backward part of the solution is a stationary contact wave from U_2^b to state U_2. The set of such states U_2^b forms the backward composite curve $\mathcal{W}_{23B}^{caseC}(U_R, a_L)$. Observe that $U_R^{@b}$ and V^{+b} are two endpoints of this curve. For example, see the red curve in Figure 3. If the curve $\mathcal{W}_1(U_L)$ intersects the curve $\mathcal{W}_{23B}^{caseC}(U_R, a_L)$ at a point U_1, then the Riemann problem of (1.1)-(1.2) admits a solution of the form

$$W_1(U_L, U_1) \oplus W_3(U_1, U_2) \oplus S_2(U_2, U_R). \tag{3.9}$$

Remark 3.9. If U_1 belongs to the rarefaction part $\mathcal{R}_1(U_L)$, then the solution (3.9) makes sense if $a_L > a_{\min}(U_R)$. If U_1 belongs to the shock part $\mathcal{S}_2(U_L)$, then the solution (3.9) makes sense if $a_L > a_{\min}(U_R)$ and $\sigma_1(U_L, U_1) < 0$.

Computational algorithm for Construction C3: We sketch to compute the point U_2, U_1 as follows.

- Step 1: Set $\rho_1 = \rho_R^{@}$, $\rho_2 = \rho^+$;
- Step 2:
  - Compute $\rho = \dfrac{\rho_1 + \rho_2}{2}$, $u = w_2^B(U_R; \rho)$ and set $U_2 = (\rho, u)$;
  - Compute $U_1 = SW^{bigger}(U_2, a_R, a_L)$;

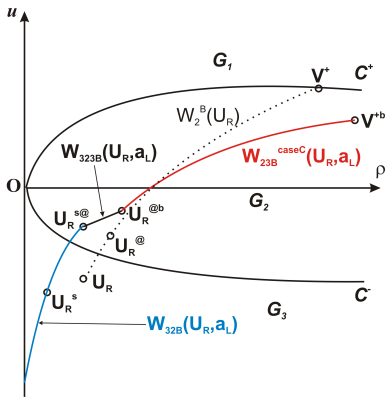

FIGURE 3. The composite wave curves $\mathcal{W}_{32B}(U_R, a_L)$, $\mathcal{W}_{323}(U_R, a_L)$ and $\mathcal{W}_{23B}^{caseC}(U_R, a_L)$ in the (ρ, u)-plane.

- Step 3:
  - If U_1 belongs to $\mathcal{W}_1(U_L)$, end;
  - If U_1 is above $\mathcal{W}_1(U_L)$, then set $\rho_2 = \rho$ and return Step 2;
  - If U_1 is below $\mathcal{W}_1(U_L)$, then set $\rho_1 = \rho$ and return Step 2.

3.4. Case D: $U_R \in G_2$

Construction D1: The Riemann solution begins backward with a 2-rarefaction wave from V^- to U_R. The next backward part of the solution is a stationary contact wave from V^{-s} to V^-. By Lemma 2.1, there is one state $V^{-s@}$ on the backward curve $\mathcal{S}_2^B(V^{-s})$ such that $\sigma_2(V^{-s@}, V^{-s}) = 0$ and $\sigma_2(U, V^{-s}) < 0$ for $\rho^{-s} < \rho < \rho^{-s@}$, $\sigma_2(U, V^{-s}) > 0$ for $\rho > \rho^{-s@}$. So, the next backward part of the solution is a 2-wave from some state $U(\rho, u)$ to V^{-s} such that $0 < \rho \le \rho^{-s@}$. The set of these states U forms the backward composite curve $\mathcal{W}_{232B}(U_R, a_L)$. Observe that $\mathcal{W}_{232B}^B(U_R, a_L)$ is a part of the curve $\mathcal{W}_2^B(V^{-s}, , a_L)$. For example, see the blue curve in Figure 4. If the curve $\mathcal{W}_1(U_L)$ intersects the curve $\mathcal{W}_{232B}(U_R, a_L)$ at a point U_1, then the Riemann problem of (1.1)-(1.2) admits a solution of the form

$$W_1(U_L, U_1) \oplus W_2(U_1, V^{-s}) \oplus W_3(V^{-s}, V^-) \oplus R_2(V^-, U_R). \tag{3.10}$$

Remark 3.10. If

$$\max\{\lambda_1(U_L), \lambda_1(U_1)\} \le \min\{\lambda_2(U_1), \lambda_2(V^{-s})\} \text{ and } a_L > a_{\min}(U_R),$$

then the solution (3.10) makes sense.

Computational algorithm for Construction D1: is similar to *Computational algorithm for Construction C1*, since the composite wave curve $\mathcal{W}_{232B}(U_R, a_L)$ concides with $\mathcal{W}_{32B}(V^-, a_L)$.

Construction D2: The Riemann solution begins backward with a 2-rarefaction wave from V^- to U_R. For each level a between a_L and a_R, the next backward part is a stationary contact wave from $V^{-s} = SW^{smaller}(V^-, a_R, a)$ to V^-. The next backward part of the solution is a 2-shock from state $V^{-s@}$ to state V^{-s}. Then, the next backward part of the solution is a stationary contact wave from $V^{-s@b} = SW^{bigger}(V^{-s@}, a, a_L)$ to $V^{-s@}$. The set of such states $V^{-s@b}$ forms the backward composite curve $\mathcal{W}_{2323B}(U_R, a_L)$. So, V^{-b} and $V^{-s@}$ are two endpoints of this curve. For example, see the black curve in Figure 4. If the curve $\mathcal{W}_1(U_L)$ intersects the curve $\mathcal{W}_{2323B}(U_R, a_L)$ at a point U_1, then the Riemann problem of (1.1)-(1.2) admits a solution of the form

$$\begin{aligned} W_1(U_L, U_1 = V^{-s@b}) \oplus W_3(U_1, V^{-s@}) \oplus S_2(V^{-s@}, V^{-s}) \\ \oplus W_3(V^{-s}, V^-) \oplus R_2(V^-, U_R). \end{aligned} \tag{3.11}$$

Remark 3.11. If U_1 belongs to the rarefaction part $\mathcal{R}_1(U_L)$, then the solution (3.11) makes sense if $a_L > a_{\min}(U_R)$. If U_1 belongs to the shock part $\mathcal{S}_2(U_L)$, then the solution (3.11) makes sense if $a_L > a_{\min}(U_R)$ and $\sigma_1(U_L, U_1) < 0$.

Computational algorithm for Construction D2: is similar to *Computational algorithm for Construction C2*, since the composite wave curve $\mathcal{W}_{2323B}(U_R, a_L)$ concides with $\mathcal{W}_{323B}(V^-, a_L)$.

Construction D3: The Riemann solution begins backward with 2-wave from U_2 to U_R such that U_2 is between V^- and V^+. The next backward part of the solution is a stationary contact wave from U_2^b to state U_2. The set of such states U_2^b forms the backward composite curve $\mathcal{W}_{23B}^{caseD}(U_R, a_L)$. Observe that V^{-b} and V^{+b} are two endpoints of this curve. For example, see the red curve in Figure 4. If the curve $\mathcal{W}_1(U_L)$ intersects the curve $\mathcal{W}_{23B}^{caseD}(U_R, a_L)$ at a point U_1, then the Riemann problem of (1.1)-(1.2) admits a solution of the form

$$W_1(U_L, U_1) \oplus W_3(U_1, U_2) \oplus W_2(U_2, U_R). \tag{3.12}$$

Remark 3.12. If U_1 belongs to the rarefaction part $\mathcal{R}_1(U_L)$, then the solution (3.12) makes sense if $a_L > a_{\min}(U_R)$. If U_1 belongs to the shock part $\mathcal{S}_2(U_L)$, then the solution (3.12) makes sense if $a_L > a_{\min}(U_R)$ and $\sigma_1(U_L, U_1) < 0$.

Computational algorithm for Construction D3: is similar to *Computational algorithm for Construction C3*, but we need to replace $\rho_1 = \rho_R^{@}$ from Step 1 with $\rho_1 = \rho^-$.

4. Building a van Leer-type scheme

Relying on the constructions of Riemann solutions in the previous section, we are now in a position to build up a van Leer-type scheme for (1.1)-(1.2). Let us set

$$U := \begin{pmatrix} \rho \\ \rho u \\ a \end{pmatrix}, \quad F(U) := \begin{pmatrix} \rho u \\ \rho u^2 + p \\ 0 \end{pmatrix}, \quad H(U) := -\frac{1}{a} \begin{pmatrix} \rho u \\ \rho u^2 \\ 0 \end{pmatrix}. \tag{4.1}$$

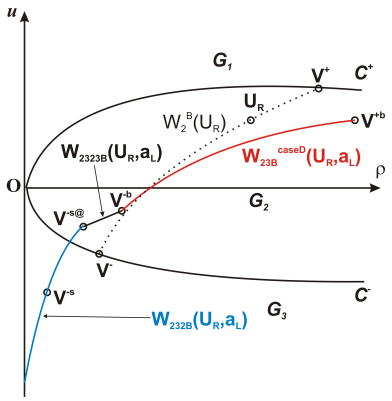

FIGURE 4. The composite wave curves $\mathcal{W}_{232B}(U_R, a_L)$, $\mathcal{W}_{2323}(U_R, a_L)$ and $\mathcal{W}_{23B}^{caseD}(U_R, a_L)$ in the (ρ, u)-plane.

Then, the system (1.1)-(1.2) can be written in form

$$\partial_t U + \partial_x F(U) = H(U)\partial_x a. \tag{4.2}$$

Accordingly, given the initial condition

$$U(x,0) = U_0(x), \quad x \in \mathbb{R}, \tag{4.3}$$

then, the discrete initial values $U^0 = (U_j^0)_{j\in\mathbb{Z}}$ are given by

$$U_j^0 := \frac{1}{\Delta x}\int_{x_{j-1/2}}^{x_{j+1/2}} U_0(x)dx, \quad j \in \mathbb{Z}. \tag{4.4}$$

Recently, the Godunov-type scheme is built in [14] as

$$U_j^{n+1} = U_j^n - \frac{\Delta t}{\Delta x}\Big(F(U_{exact}(0-; U_j^n, U_{j+1}^n)) - F(U_{exact}(0+; U_{j-1}^n, U_j^n))\Big), \tag{4.5}$$

where $U_{exact}\Big(\frac{x}{t}; U_L, U_R\Big)$ denote the exact solution of the Riemann problem for (4.2) corresponding to the Riemann data (U_L, U_R). Now, in this paper, we build a van Leer-type scheme as follows.

Suppose $U^n = (U_j^n)_{j\in\mathbb{Z}}$ at the time t_n is known. We define the approximation $U^{n+1} = (U_j^{n+1})_{j\in\mathbb{Z}}$ of $U(\cdot, t_{n+1})$ as follows:

(i) From the sequence U^n, we construct a piecewise linear function $U_{p.lin}(\cdot, t_n)$ defined by

$$U_{p.lin}(x, t_n) = U_j^n + \frac{S_j^n}{\Delta x}(x - x_j), \quad x_{j-1/2} < x < x_{j+1/2}, \quad j \in \mathbb{Z}, \tag{4.6}$$

where the slopes S_j^n are defined by

$$\begin{aligned} S_j^n &= (U_{j+1}^n - U_j^n)\Phi(\theta_j^n), \\ \theta_j^n &= \frac{U_j^n - U_{j-1}^n}{U_{j+1}^n - U_j^n}, \\ \Phi(\theta) &= \frac{|\theta| + \theta}{1 + |\theta|}, \quad \textit{the van Leer's limiter function.} \end{aligned} \tag{4.7}$$

(ii) We solve the Cauchy problem for (4.2) with the initial condition

$$U(x, 0) = U_{p.lin}(x, t_n), \tag{4.8}$$

to find the solution $U(\cdot, \Delta t)$.

(iii) We project (in the sense of $\mathbb{L}^2$) the solution $U(\cdot, \Delta t)$ onto the piecewise constant funtions, i.e., we set

$$U_j^{n+1} := \frac{1}{\Delta x} \int_{x_{j-1/2}}^{x_{j+1/2}} U(x, \Delta t) dx. \tag{4.9}$$

Provided we assume some C.F.L. condition so that the waves issued from the points $x_{j-1/2}$ and $x_{j+1/2}$ do not interact, the solution is obtained by juxtaposition of local Riemann problems

$$\frac{\Delta t}{\Delta x} \max\{|\lambda_k(U_j^n)| : k = 1, 2\} \leq C.F.L. \tag{4.10}$$

In order to derive a more explicit form of the scheme, we intergrate the equation (4.2) over the rectangle $(x_{j-1/2}, x_{j+1/2}) \times (0, \Delta t)$. Since a is constant on $(x_{j-1/2}, x_{j+1/2})$, we obtain

$$\begin{aligned} &\int_{x_{j-1/2}}^{x_{j+1/2}} (U(x, \Delta t) - U(x, 0)) dx \\ &+ \int_0^{\Delta t} \Big(F(U(x_{j+1/2} - 0, t)) - F(U(x_{j-1/2} + 0, t)) \Big) dt = 0. \end{aligned} \tag{4.11}$$

Using (4.6), (4.8) and (4.9), we get

$$\Delta x(U_j^{n+1} - U_j^n) + \int_0^{\Delta t} \Big(F(U(x_{j+1/2} - 0, t)) - F(U(x_{j-1/2} + 0, t)) \Big) dt = 0. \tag{4.12}$$

Using the midpoint rule, we write

$$\begin{aligned} \frac{1}{\Delta t} \int_0^{\Delta t} F(U(x_{j+1/2} - 0, t)) dt &= F(U(x_{j+1/2} - 0, \Delta t/2)) + O(\Delta t^2), \\ \frac{1}{\Delta t} \int_0^{\Delta t} F(U(x_{j-1/2} + 0, t)) dt &= F(U(x_{j-1/2} + 0, \Delta t/2)) + O(\Delta t^2). \end{aligned} \tag{4.13}$$

For approximating $F(U(x_{j+1/2} - 0, \Delta t/2))$ and $F(U(x_{j-1/2} + 0, \Delta t/2))$, we use a predictor-corrector scheme. First, following an idea of Hancock, we define

the updated values $U^{n+1/2}_{j+1/2,\pm}$ at time $t_n + \Delta t/2$ by

$$\begin{aligned} U^{n+1/2}_{j+1/2,-} &= U^n_{j+1/2,-} - \frac{\Delta t}{2\Delta x}(F(U^n_{j+1/2,-}) - F(U^n_{j-1/2,+})), \\ U^{n+1/2}_{j+1/2,+} &= U^n_{j+1/2,+} - \frac{\Delta t}{2\Delta x}(F(U^n_{j+3/2,-}) - F(U^n_{j+1/2,+})), \end{aligned} \tag{4.14}$$

where

$$\begin{aligned} U^n_{j+1/2,-} &= U_{p.lin}(x_{j+1/2} - 0) = U^n_j + \frac{1}{2}S^n_j, \\ U^n_{j+1/2,+} &= U_{p.lin}(x_{j+1/2} + 0) = U^n_{j+1} - \frac{1}{2}S^n_j. \end{aligned} \tag{4.15}$$

Second, we solve the Riemann problem of (4.2) at the point $x_{j+1/2}$ with piecewise constant initial data $U^{n+1/2}_{j+1/2,\pm}$, whose solution is noted as usual

$$U_{exact}\Big(\frac{x - x_{j+1/2}}{t}; U^{n+1/2}_{j+1/2,-}, U^{n+1/2}_{j+1/2,+}\Big).$$

Third, we replace $U(x_{j+1/2} \pm 0, \Delta t/2)$ by

$$U_{exact}\Big(0\pm; U^{n+1/2}_{j+1/2,-}, U^{n+1/2}_{j+1/2,+}\Big).$$

Thus, the scheme (4.12) becomes

$$U^{n+1}_j = U^n_j - \frac{\Delta t}{\Delta x}\Big(F(U_{exact}(0-, U^{n+1/2}_{j+1/2,-}, U^{n+1/2}_{j+1/2,+})) - F(U_{exact}(0+, U^{n+1/2}_{j-1/2,-}, U^{n+1/2}_{j-1/2,+}))\Big). \tag{4.16}$$

The scheme (4.16) is capable of capturing stationary waves exactly. This means that for any stationary wave, it holds that

$$U^{n+1}_j = U^n_j, \quad j \in \mathbb{Z}, \quad n = 0, 1, 2, \ldots. \tag{4.17}$$

Therefore, it is a *well-balanced scheme*. To see this, we first suppose that U^n corresponds to a stationary wave. From (4.7), we imply

$$S^n_j = 0, \quad j \in \mathbb{Z}.$$

Then, we get from (4.14), (4.15)

$$\begin{aligned} U^{n+1/2}_{j+1/2,-} &= U^n_{j+1/2,-} = U^n_j, \\ U^{n+1/2}_{j+1/2,+} &= U^n_{j+1/2,+} = U^n_{j+1}. \end{aligned}$$

Therefore, it holds that

$$U_{exact}\Big(0-; U^{n+1/2}_{j+1/2,-}, U^{n+1/2}_{j+1/2,+}\Big) = U^n_j = U_{exact}\Big(0+; U^{n+1/2}_{j-1/2,-}, U^{n+1/2}_{j-1/2,+}\Big),$$

which yield (4.17).

To complete the van Leer-type scheme (4.16), we will specify the values

$$\begin{aligned} U_{left} &:= U_{exact}\Big(0-; U_L, U_R\Big), \\ U_{right} &:= U_{exact}\Big(0+; U_L, U_R\Big), \end{aligned} \tag{4.18}$$

TABLE 1. The Riemann initial data in each test.

Test	p_L	u_L	a_L	p_R	u_R	a_R	Domain
1	0.4027329	-2.3539815	1.5	1.0	-2.0	1.0	$U_L \in G_3, U_R \in G_3$
2	5.0	2.0	2.0	2.0	2.900031	2.0	$U_L \in G_1, U_R \in G_1$
3	7.0	2.372451	2.5	5.0	2.0	2.5	$U_L \in G_1, U_R \in G_1$
4	40.0	-3.0	1.5	1.0	-2.0	1.0	$U_L \in G_3, U_R \in G_3$
5	5.0	0.5	1.5	9.0	1.0	2.5	$U_L \in G_2, U_R \in G_2$
6	3.0	1.0	1.5	5.0	2.0	2.5	$U_L \in G_2, U_R \in G_1$
7	2.0	-6.0	1.5	4.0	-1.0	1.0	$U_L \in G_3, U_R \in G_2$
8	3.5	-3.0	1.5	1.0	1.0	1.0	$U_L \in G_3, U_R \in G_2$
9	3.0	2.0	2.0	20.0	2.0	3.0	$U_L \in G_1, U_R \in G_2$

as follows.

- For Construction A1 (3.1): $U_{left} = U_L, \quad U_{right} = U_L^s$.
- For Construction A2 (3.2): $U_{left} = U_L, \quad U_{right} = U_1 = U_L^{s\#b}$.
- For Construction A3 (3.3): $U_{left} = U_1, \quad U_{right} = U_2$.
- For Construction B1 (3.4): $U_{left} = U^+, \quad U_{right} = U^{+s}$.
- For Construction B2 (3.5): $U_{left} = U^+, \quad U_{right} = U_1 = U^{+s\#b}$.
- For Construction B3 (3.6): $U_{left} = U_1, \quad U_{right} = U_2$.
- For Construction C1 (3.7): $U_{left} = U_R^s, \quad U_{right} = U_R$.
- For Construction C2 (3.8): $U_{left} = U_1 = U_R^{s@b}, \quad U_{right} = U_R$.
- For Construction C3 (3.9): $U_{left} = U_1, \quad U_{right} = U_2$.
- For Construction D1 (3.10): $U_{left} = V^{-s}, \quad U_{right} = V^-$.
- For Construction D2 (3.11): $U_{left} = U_1 = V^{-s@b}, \quad U_{right} = V^-$.
- For Construction D3 (3.12): $U_{left} = U_1, \quad U_{right} = U_2$.

5. Numerical experiments

This section is devoted to numerical tests by using MATLAB/OCTAVE. For each test, we compare the numerical solution U_h with the corresponding exact solution U. By taking

$$\kappa = 1, \quad \gamma = 1.4$$

we plot the solutions U_h and U for $t = 0.1$. The Riemann initial data in each test is given in table 1.

5.1. Test case for well-balanced property

Test 1: Consider the Riemann problem for (1.1) with the initial data given in Table 1. It is not difficult to check that the initial data of this test satisfies the jump relations (2.7). Therefore, the solution is just a contact stationary wave from U_L to U_R. Figure 5 displays an exact contact stationary wave and its approximation with 250 mesh points by the van Leer-type scheme (4.16) of Test 1. This figure shows that the van Leer-type scheme (4.16) can capture contact stationary solutions, so it is well-balanced. Moreover, the L^1-error of this test is exactly equal to zero.

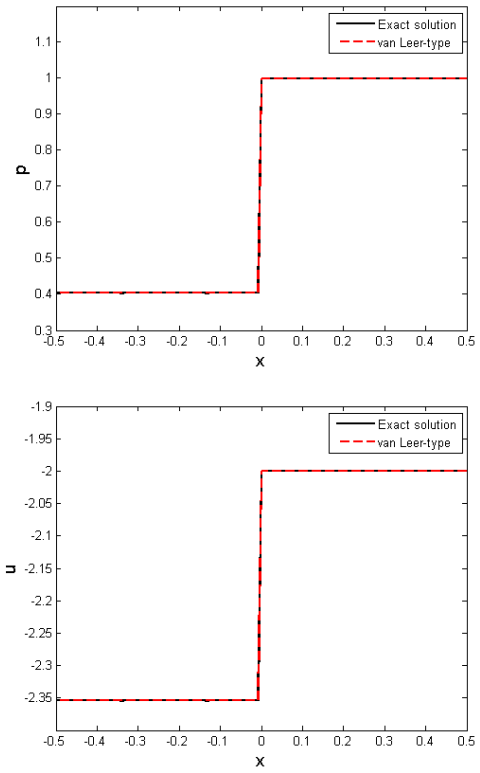

FIGURE 5. Test 1: Exact solution and approximate solutions for the mesh size $h = 1/250$.

5.2. Test for simple waves

Test 2: Consider the Riemann problem for (1.1) with the initial data given in Table 1, where U_L and U_R are located in G_1. The exact solution in this test is just a 1-rafaction wave connecting from the left-hand state U_L to the right-hand state U_R. Note that a k-rarefaction wave is a merely continuous piecewise differentiable self-similar solution. A k-rarefaction wave is not, in general, differentiable along the half straight lines $x = \lambda_k(U_\pm)t$, where $U_\pm$ are the left-hand and right-hand states. The exact and approximate solutions are displayed by Figure 6.

The errors, orders of convergence of the Godunov-type scheme and the van Leer-type scheme in this test are reported by Table 2. We could see that the order of convergence of the Godunov-type scheme is approximately equal to 2/3, while the one of the van Leer-type scheme is approximately equal to

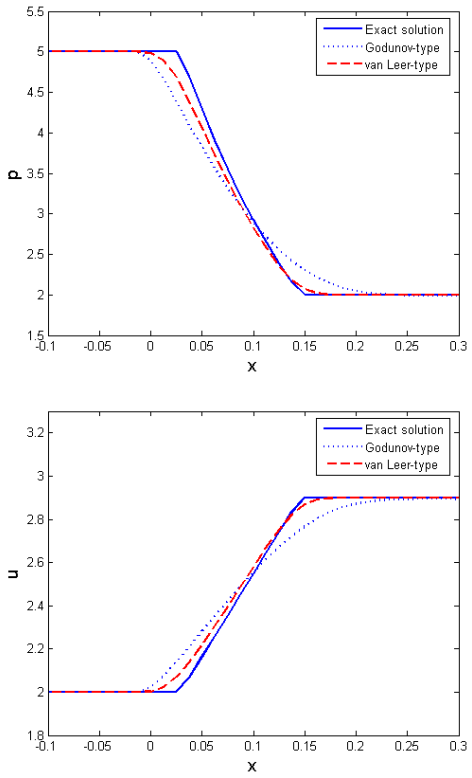

FIGURE 6. Test 2: Exact solution and approximate solutions for the mesh size $h = 1/80$ corresponding to the Godunov-type scheme and the van Leer-type scheme.

1 for a rarefaction wave. This is consistent with the fact that the "second-order" van Leer scheme for the usual gas dynamics equations has the order of convergence approximately equal to 2/3 for a contact discontinuity, and the order of convergence approximately equal to 1 for a single shock wave, see [11], for example.

Test 3: Consider the Riemann problem for (1.1) with the initial data located in G_1. The exact solution in this test is just a 2-shock wave connecting from the left-hand state U_L to the right-hand state U_R. The exact and approximate solutions are displayed by Figure 7.

The errors, orders of convergence are reported by Table 3. We can see from Table 3 that the order of convergence of the van Leer-type scheme for a shock wave is approximately equal to 4/5. This is better than the standard van Leer

TABLE 2. Errors and orders of convergence for Test 2.

	Godunov-type scheme			**van Leer-type scheme**		
N	L^1-error	L^1-relative error	Order	L^1-error	L^1-relative error	Order
20	0.21405	0.017770	–	0.18064	0.014996	–
40	0.18697	0.015507	0.20	0.12015	0.009965	0.59
80	0.11905	0.009868	0.65	0.06017	0.004988	1.00
160	0.07434	0.006163	0.68	0.02904	0.002408	1.05
320	0.04693	0.003891	0.66	0.014703	0.001219	0.98
640	0.02886	0.002393	0.70	0.00733	0.000607	1.00

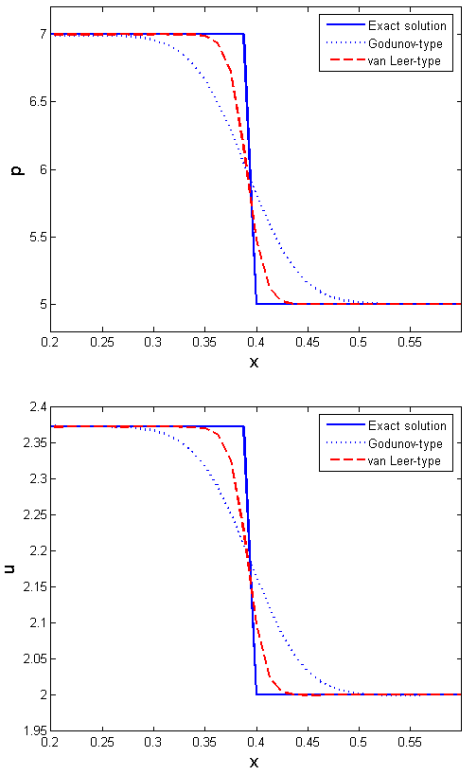

FIGURE 7. Test 3: Exact solution and approximate solutions for the mesh size $h = 1/80$ corresponding to the Godunov-type scheme and the van Leer-type scheme.

scheme for the usual gas dynamics equations for a contact discontinuity (order 2/3), but worse than the one for a shock wave (order 1).

TABLE 3. Errors and orders of convergence for Test 3.

	Godunov-type scheme			**van Leer-type scheme**		
N	L^1-error	L^1-relative error	Order	L^1-error	L^1-relative error	Order
20	0.26161	0.015173	–	0.15265	0.008853	–
40	0.18215	0.010540	0.52	0.09105	0.005268	0.75
80	0.12502	0.007226	0.54	0.05238	0.003027	0.80
160	0.08379	0.004840	0.58	0.02920	0.001687	0.84
320	0.05486	0.003168	0.61	0.01673	0.000966	0.80
640	0.03403	0.001966	0.69	0.00697	0.000403	1.26

TABLE 4. States that separate the elementary waves of the exact solution of the Riemann problem in Test 4.

	U_1	U_2
p	5.0270365	4.8773098
u	-0.2871028	-0.4388701
a	1.5	1.0

Since the system (1.1) contains a *nonconservative term* pa_x, the results in Tests 2 and 3 show that the accuracy of our van Leer-type scheme reasonable in comparing with the standard van Leer scheme for a single wave.

5.3. Test cases for a complete Riemann solution when initial data either belongs to subsonic or supersonic region

Test 4: In this test, we consider the Riemann initial data in the line test 4 in Table 1, where U_L, U_R are in the same region G_3. According to the Construction C3, the exact solution is a 1-rarefaction wave from U_L to U_1, followed by a stationary wave from U_1 to U_2, then followed by a 2-shock wave from U_2 to U_R, where U_1, U_2 are reported in Table 4. Figure 8 displays the exact solution and its approximate solutions for the mesh size $h = 1/1000$ corresponding to the Godunov-type scheme and the van Leer-type scheme. One can see from this figure that the approximate solutions are closed to the exact solution. The errors, orders of convergence are reported by Table 5. Moreover, Table 5 shows that the accuracy of the van Leer-type scheme are better than the Godunov-type scheme.

Test 5: In this test, the initial data U_L, U_R belong to subsonic region G_2. According to Construction B3, the exact solution is a 1-rarefaction wave from U_L to U_1, followed by a stationary wave from U_1 to U_2, then followed by a 2-rarefaction wave from U_2 to U_R, where U_1, U_2 are reported in Table 6. Figure 9 displays the exact solution and its approximate solutions for the mesh size $h = 1/1000$ corresponding to the Godunov-type scheme and the van Leer-type scheme. One can see from this figure that the approximate solutions are closed to the exact solution. The errors, orders of convergence are reported by Table

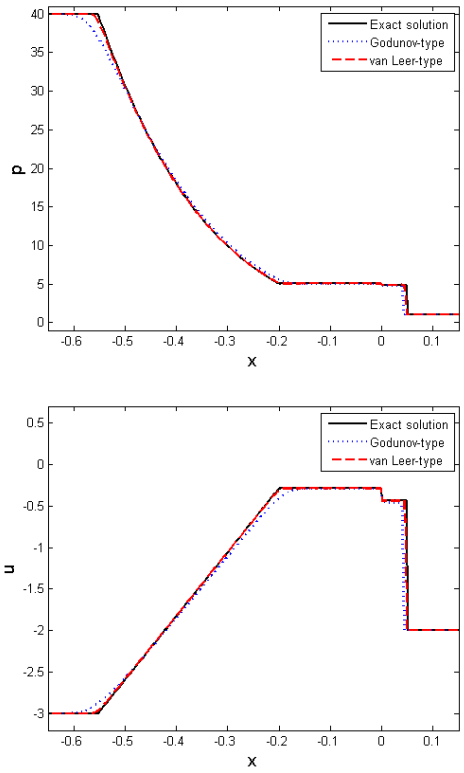

FIGURE 8. Test 4: Exact solution and approximate solutions for the mesh size $h = 1/1000$ corresponding to the Godunov-type scheme and the van Leer-type scheme.

TABLE 5. Errors and orders of convergence for Test 4.

	Godunov-type scheme			**van Leer-type scheme**		
N	L^1-error	L^1-relative error	Order	L^1-error	L^1-relative error	Order
125	1.36680	0.045148	–	0.34020	0.011238	–
250	0.88913	0.029317	0.62	0.25517	0.008414	0.41
500	0.53575	0.017671	0.73	0.11868	0.003915	1.10
1000	0.32367	0.010676	0.73	0.05812	0.001917	1.03

7. Moreover, Table 7 shows that the accuracy and the order of convergence of the van Leer-type scheme are better than the Godunov-type scheme.

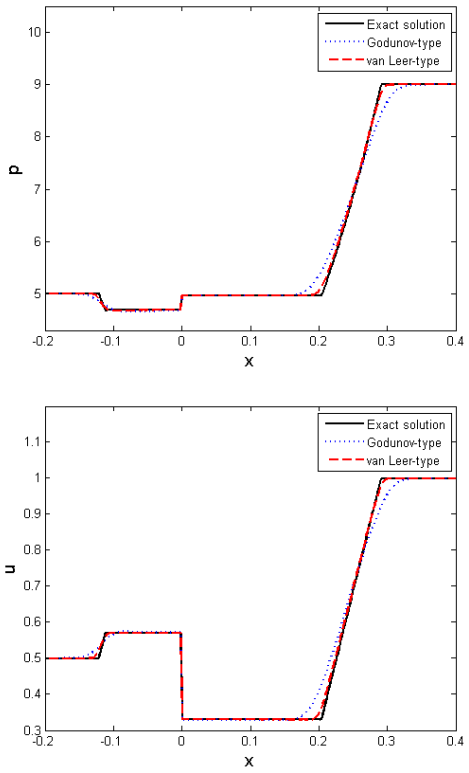

FIGURE 9. Test 5: Exact solution and approximate solutions for the mesh size $h = 1/1000$ corresponding to the Godunov-type scheme and the van Leer-type scheme.

TABLE 6. States that separate the elementary waves of the exact solution of the Riemann problem in Test 5.

	U_1	U_2
p	4.6813575	4.9706328
u	0.5699637	0.3294000
a	1.5	2.5

5.4. Test cases for initial data in different regions without resonance (no wave collisions)

Test 6: The initial data of this test is the line test 6 in Table 1, where $U_L \in G_2$, $U_R \in G_1$. According to the Construction B1, the exact solution is a 1-rarefaction wave from U_L to U^+, followed by a stationary wave from U^+ to U_1,

TABLE 7. Errors and orders of convergence for Test 5.

	Godunov-type scheme			**van Leer-type scheme**		
N	L^1-error	L^1-relative error	Order	L^1-error	L^1-relative error	Order
125	0.16113	0.011399	–	0.05759	0.004074	–
250	0.10999	0.007695	0.55	0.03639	0.002546	0.66
500	0.07145	0.004999	0.62	0.01856	0.001299	0.97
1000	0.04565	0.003194	0.65	0.00923	0.000646	1.01

TABLE 8. States that separate the elementary waves of the exact solution of the Riemann problem in Test 6.

	U^+	U_1	U_2
p	1.8976227	0.4077600	1.8160209
u	1.4263449	2.2374542	1.4263449
a	1.5	2.5	2.5

TABLE 9. Errors and orders of convergence for Test 6.

	Godunov-type scheme			**van Leer-type scheme**		
N	L^1-error	L^1-relative error	Order	L^1-error	L^1-relative error	Order
125	0.17492	0.018307	–	0.062524	0.006544	–
250	0.11102	0.011488	0.66	0.037210	0.003850	0.75
500	0.071309	0.007377	0.64	0.023354	0.002416	0.67
1000	0.046281	0.004787	0.62	0.014887	0.001540	0.65

followed by a 1-shock wave from U_1 to U_2, then followed by a 2-rarefaction wave from U_2 to U_R, where U^+, U_1, U_2 are reported in Table 8. Figure 10 displays the exact solution and its approximate solutions for the mesh size $h = 1/1000$ corresponding to the Godunov-type scheme and the van Leer-type scheme. We can see from this figure that the approximate solutions are closed to the exact solution. The errors, orders of convergence are reported by Table 9. Moreover, Table 9 shows that the accuracy of the van Leer-type scheme is much better than the Godunov-type scheme.

Test 7: In this test, we consider the initial data on the line test 7 of Table 1, where $U_L \in G_3$, $U_R \in G_2$. According the Construction D1, the exact solution is a 1-rarefaction wave from U_L to U_1, followed by a 2-rarefaction wave from U_1 to U_2, followed by a stationary wave from U_2 to V^-, then followed by a 2-rarefaction wave from V^- to U_R, where V^-, U_1, U_2 are reported in Table 10. Figure 11 displays the exact solution and its approximate solutions for the mesh size $h = 1/1000$ corresponding to the Godunov-type scheme and the van Leer-type scheme. We can see from this figure that the approximate solutions are closed to the exact solution. The errors, orders of convergence are reported by Table 11. Table 11 shows that the accuracy of the van Leer-type scheme is

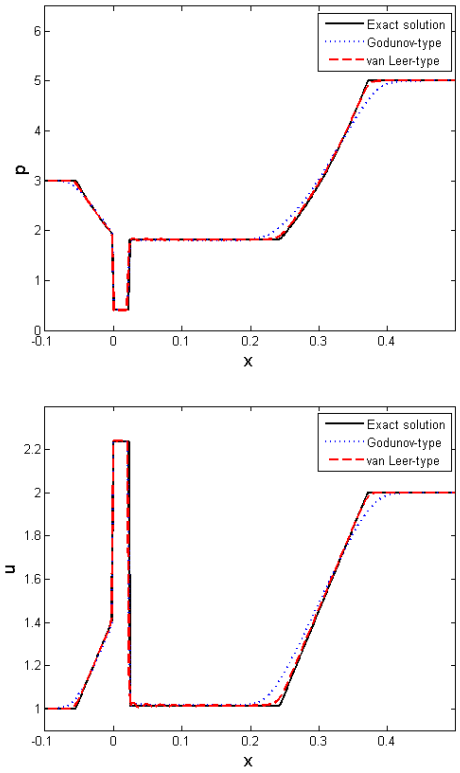

FIGURE 10. Test 6: Exact solution and approximate solutions for the mesh size $h = 1/1000$ corresponding to the Godunov-type scheme and the van Leer-type scheme.

TABLE 10. States that separate the elementary waves of the exact solution of the Riemann problem in Test 7.

	U_1	U_2	V^-
p	0.0585128	0.6497368	2.4176117
u	-3.6747174	-2.2620867	-1.4926048
a	1.5	1.5	1.0

much better than the Godunov-type scheme. Moreover, when the order of the Godunov-type scheme seems to be unstable at $N = 250$, the one of the van Leer-type scheme is still stable.

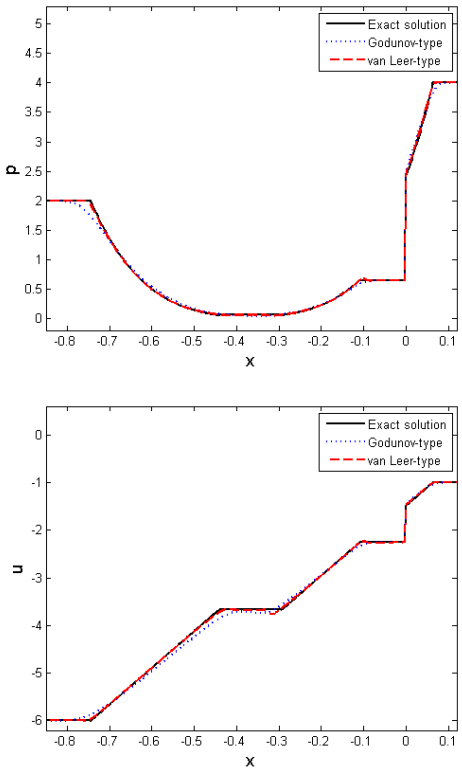

FIGURE 11. Test 7: Exact solution and approximate solutions for the mesh size $h = 1/1000$ corresponding to the Godunov-type scheme and the van Leer-type scheme.

TABLE 11. Errors and orders of convergence for Test 7.

	Godunov-type scheme			**van Leer-type scheme**		
N	L^1-error	L^1-relative error	Order	L^1-error	L^1-relative error	Order
125	3.02320	0.300650	–	0.10884	0.010824	–
250	3.01810	0.297680	0.00	0.05860	0.005780	0.89
500	0.12360	0.012195	4.61	0.03134	0.003093	0.90
1000	0.07678	0.007576	0.69	0.01572	0.001551	1.00

5.5. Test cases for resonance

Test 8: We consider the Riemann initial data in the line test 8 in Table 1, where $U_L \in G_3$, $U_R \in G_2$. According to the Construction D2, the exact solution is a 1-rarefaction wave from U_L to U_1, followed by a stationary wave from U_1

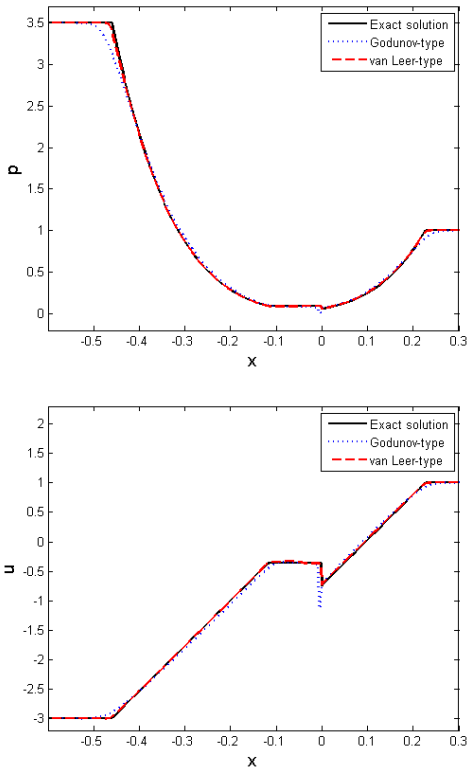

FIGURE 12. Test 8: Exact solution and approximate solutions for the mesh size $h = 1/1000$ corresponding to the Godunov-type scheme and the van Leer-type scheme.

to U_2, followed by a 2-shock which has zero speed from U_2 to U_3, followed again by a stationary from U_3 to V^-, then followed by a 2-rarefaction from V^- to U_R, where V^-, U_1, U_2, U_3 are reported in Table 12. Figure 12 displays the exact solution and its approximate solutions for the mesh size $h = 1/1000$ corresponding to the Godunov-type scheme and the van Leer-type scheme. This figure illustrates good approximations to the exact solution. The errors and orders of convergence for this test are reported in the Table 13, where one can see that the accuracy of the van Leer-type scheme is much better than the Godunov-type scheme.

Test 9: In this test, we approximate the Riemann solution of Construction A2, where the initial data $U_1 \in G_1$, $U_R \in G_2$ are given in Table 1. The exact solution is a stationary wave from U_L to U_1, followed by a 1-shock which has zero speed from U_1 to U_2, followed again by a stationary from U_2 to U_3, then

TABLE 12. States that separate the elementary waves of the exact solution of the Riemann problem in Test 8.

	U_1	U_2	U_3	V^-
p	0.0931348	0.0783748	0.0279140	0.0582436
u	-0.3690093	-0.5228519	-0.9967824	-0.7422390
a	1.5	1.1791916	1.1791916	1.0

TABLE 13. Errors and orders of convergence for Test 8.

	Godunov-type scheme			**van Leer-type scheme**		
N	L^1-error	L^1-relative error	Order	L^1-error	L^1-relative error	Order
125	0.30204	0.048571	–	0.08526	0.013711	–
250	0.18778	0.030037	0.69	0.04966	0.007944	0.78
500	0.11443	0.018307	0.71	0.02609	0.004174	0.93
1000	0.06784	0.010854	0.75	0.01281	0.002049	1.03

TABLE 14. States that separate the elementary waves of the exact solution of the Riemann problem in Test 9.

	U_1	U_2	U_3
p	2.5840830	5.7382918	7.4728266
u	2.1067208	1.2795562	0.7537225
a	2.0843097	2.0843097	3.0

TABLE 15. Errors and orders of convergence for Test 9.

	Godunov-type scheme			**van Leer-type scheme**		
N	L^1-error	L^1-relative error	Order	L^1-error	L^1-relative error	Order
125	0.47251	0.021643	–	0.12187	0.005582	–
250	0.31645	0.014261	0.58	0.083965	0.003784	0.54
500	0.20079	0.009054	0.66	0.042581	0.001920	0.98
1000	0.12441	0.005610	0.69	0.021262	0.000959	1.00

followed by a 2-rarefaction wave from U_3 to U_R, where U_1, U_2, U_3 are reported in Table 14. Figure 13 displays the exact solution and its approximate solutions for the mesh size $h = 1/1000$ corresponding to the Godunov-type scheme and the van Leer-type scheme. This figure illustrates good approximations to the exact solution. The errors and order of convergence for Test 9 are reported in the Table 15, where one can see that the accuracy and the order of convergence of the van Leer-type scheme are better than the Godunov-type scheme.

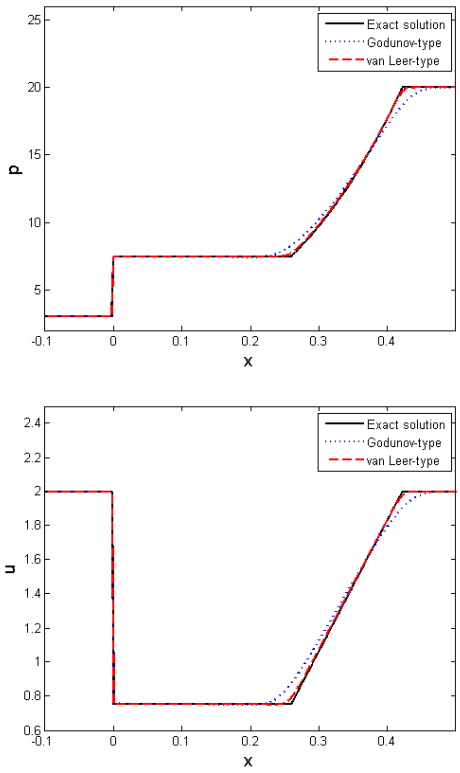

FIGURE 13. Test 9: Exact solution and approximate solutions for the mesh size $h = 1/1000$ corresponding to the Godunov-type scheme and the van Leer-type scheme.

6. Conclusions and discussions

We successfully build a van Leer-type scheme for the isentropic model of fluid flows in a nozzle with variable cross-section (1.1). The scheme possesses a good accuracy, and is well-balanced. Tests show that this van Leer-type scheme can give good approximations for exact solutions not only when the initial data are located in each subsonic or supersonic region, but also in both regions. Especially, the scheme can approximate very well the exact solution in the resonant case, where the exact solution contains colliding waves. This is a nice advantage over many existing schemes.

The van-Leer type scheme has a much better accuracy than the Godunov-type scheme. This is consistent with the standard Godunov's and van Leer schemes for the usual gas dynamics equations. However, the question on the efficiency of the method still remains.

Acknowledgements. The authors would like to thank the reviewers for their very constructive comments and fruitful discussions.

References

[1] A. Ambroso, C. Chalons, F. Coquel, and T. Galié, *Relaxation and numerical approximation of a two-fluid two-pressure diphasic model*, Math. Mod. Numer. Anal. **43** (2009), no. 6, 1063–1097.

[2] A. Ambroso, C. Chalons, and P.-A. Raviart, *A Godunov-type method for the seven-equation model of compressible two-phase flow*, Comput. & Fluids **54** (2012), 67–91.

[3] E. Audusse, F. Bouchut, M.-O. Bristeau, R. Klein, and B. Perthame, *A fast and stable well-balanced scheme with hydrostatic reconstruction for shallow water flows*, SIAM J. Sci. Comput. **25** (2004), no. 6, 2050–2065.

[4] M. Baudin, F. Coquel, and Q.-H. Tran, *A semi-implicit relaxation scheme for modeling two-phase flow in a pipeline*, SIAM J. Sci. Comput. **27** (2005), no. 3, 914–936.

[5] M. Ben-Artzi and J. Falcovitz, *An Upwind Second-Order Scheme for Compressible Duct Flows*, SIAM J. Sci. and Stat. Comput. **7** (1986), 744–768.

[6] R. Botchorishvili, B. Perthame, and A. Vasseur, *Equilibrium schemes for scalar conservation laws with stiff sources*, Math. Comp. **72** (2003), no. 241, 131–157.

[7] R. Botchorishvili and O. Pironneau, *Finite volume schemes with equilibrium type discretization of source terms for scalar conservation laws*, J. Comput. Phys. **187** (2003), no. 2, 391–427.

[8] A. Chinnayya, A.-Y. LeRoux, and N. Seguin, *A well-balanced numerical scheme for the approximation of the shallow water equations with topography: the resonance phenomenon*, Int. J. Finite **1** (2004), no. 4, 1–33.

[9] C. E. Castro and E. F. Toro, *A Riemann solver and upwind methods for a two-phase flow model in non-conservative form*, Internat. J. Numer. Methods Fluids **50** (2006), no. 3, 275–307.

[10] F. Coquel, K. El Amine, E. Godlewski, B. Perthame, and P. Rascle, *A numerical method using upwind schemes for the resolution of two-phase flows*, J. Comput. Phys. **136** (1997), no. 2, 272–288.

[11] F. Coquel, P. Helluy, and J. Schneider, *Second-order entropy diminishing scheme for the Euler equations*, Int. J. Num. Meth. Fluids **50** (2006), no. 9, 1029–1061.

[12] F. Coquel, J.-M. Hérard, K. Saleh, and N. Seguin, *Two properties of two-velocity two-pressure models for two-phase flows*, Commun. Math. Sci. **12** (2014), no. 3, 593–600.

[13] F. Coquel, K. Saleh, and N. Seguin, *A robust and entropy-satisfying numerical scheme for fluid flows in discontinuous nozzles*, Math. Models Methods Appl. Sci. **24** (2014), no. 10, 2043–2083.

[14] D. H. Cuong and M. D. Thanh, *A Godunov-type scheme for the isentropic model of a fluid flow in a nozzle with variable cross-section*, Appl. Math. Comput. **256** (2015), 602–629.

[15] G. Dal Maso, P. G. LeFloch, and F. Murat, *Definition and weak stability of nonconservative products*, J. Math. Pures Appl. **74** (1995), no. 6, 483–548.

[16] T. Gallouët, J.-M. Hérard, and N. Seguin, *Numerical modeling of two-phase flows using the two-fluid two-pressure approach*, Math. Models Methods Appl. Sci. **14** (2004), no. 5, 663–700.

[17] P. Goatin and P. G. LeFloch, *The Riemann problem for a class of resonant nonlinear systems of balance laws*, Ann. Inst. H. Poincaré Anal. Non Linéaire **21** (2004), no. 6, 881–902.

[18] J. M. Greenberg and A. Y. Leroux, *A well-balanced scheme for the numerical processing of source terms in hyperbolic equations*, SIAM J. Numer. Anal. **33** (1996), no. 1, 1–16.

[19] E. Isaacson and B. Temple, *Nonlinear resonance in systems of conservation laws*, SIAM J. Appl. Math. **52** (1992), no. 5, 1260–1278.
[20] ———, *Convergence of the* 2×2 *Godunov method for a general resonant nonlinear balance law*, SIAM J. Appl. Math. **55** (1995), no. 3, 625–640.
[21] B. L. Keyfitz, R. Sander, and M. Sever, *Lack of hyperbolicity in the two-fluid model for two-phase incompressible flow*, Discrete Contin. Dyn. Sys. Ser. B **3** (2003), no. 4, 541–563.
[22] D. Kröner, P. G. LeFloch, and M. D. Thanh, *The minimum entropy principle for compressible fluid flows in a nozzle with discontinuous cross-section*, M2AN Math. Model. Numer. Anal. **42** (2008), no. 3, 425–442.
[23] D. Kröner and M. D. Thanh, *Numerical solutions to compressible flows in a nozzle with variable cross-section*, SIAM J. Numer. Anal. **43** (2005), no. 2, 796–824.
[24] P. G. LeFloch and M. D. Thanh, *The Riemann problem for fluid flows in a nozzle with discontinuous cross-section*, Commun. Math. Sci. **1** (2003), no. 4, 763–797.
[25] ———, *The Riemann problem for the shallow water equations with discontinuous topography*, Commun. Math. Sci. **5** (2007), no. 4, 865–885.
[26] ———, *A Godunov-type method for the shallow water equations with discontinuous topography in the resonant regime*, J. Comput. Phys. **230** (2011), no. 20, 7631–7660.
[27] D. Marchesin and P. J. Paes-Leme, *A Riemann problem in gas dynamics with bifurcation*, Hyperbolic partial differential equations, III. Comput. Math. Appl. Part A **12** (1986), no. 4-5, 433–455.
[28] S. T. Munkejord, *Comparison of Roe-type methods for solving the two-fluid model with and without pressure relaxation*, Computers & Fluids **36** (2007), 1061–1080.
[29] R. Saurel and R. Abgrall, *A multiphase Godunov method for compressible multifluid and multiphase flows*, J. Comput. Phys. **150** (1999), 425–467.
[30] D. W. Schwendeman, C. W. Wahle, and A. K. Kapila, *The Riemann problem and a high-resolution Godunov method for a model of compressible two-phase flow*, J. Comput. Phys. **212** (2006), 490–526.
[31] M. D. Thanh, *The Riemann problem for a non-isentropic fluid in a nozzle with discontinuous cross-sectional area*, SIAM J. Appl. Math. **69** (2009), 1501–1519.
[32] ———, *A phase decomposition approach and the Riemann problem for a model of two-phase flows*, J. Math. Anal. Appl. **418** (2014), no. 2, 569–594.
[33] ———, *Well-balanced Roe-type numerical scheme for a model of two-phase compressible flows*, J. Korean Math. Soc. **51** (2014), no. 1, 163–187.
[34] M. D. Thanh and D. H. Cuong, *Existence of solutions to the Riemann problem for a model of two-phase flows*, Electron. J. Differential Equations **2015** (2015), no. 32, 1–18.
[35] M. D. Thanh, D. Kröner, and C. Chalons, *A robust numerical method for approximating solutions of a model of two-phase flows and its properties*, Appl. Math. Comput. **219** (2012), no. 1, 320–344.
[36] M. D. Thanh, D. Kröner, and N. T. Nam, *Numerical approximation for a Baer-Nunziato model of two-phase flows*, Appl. Numer. Math. **61** (2011), no. 5, 702–721.

Dao Huy Cuong
Nguyen Huu Cau High School
07 Nguyen Anh Thu, Trung Chanh Ward, Hoc Mon District
and
Department of Mathematics and Computer Science
University of Science (VNU-HCM)
227 Nguyen Van Cu str., District 5, Ho Chi Minh City, Vietnam
E-mail address: cuongnhc82@gmail.com

Mai Duc Thanh
Department of Mathematics
International University (VNU-HCM)
Quarter 6, Linh Trung Ward, Thu Duc District, Ho Chi Minh City, Vietnam
E-mail address: mdthanh@hcmiu.edu.vn